Contract No:

This document was prepared in conjunction with work accomplished under Contract No. DE-AC09-08SR22470 with the U.S. Department of Energy (DOE) Office of Environmental Management (EM).

Disclaimer:

SRNL-STI-2018-00187

Proceedings of the ASME 2018 Pressure Vessels and Piping Conference
PVP2018
July 15-20, 2018, Prague, Czech Republic

Draft PVP2018-84755

IMAGING HYDROGEN IN STAINLESS STEEL ALLOYS BY KELVIN PROBE FORCE MICROSCOPY†

J. D. McNamara‡ **A. J. Duncan**
M. J. Morgan **P. S. Korinko**
Materials Science and Technology
Savannah River National Laboratory
Aiken, South Carolina 29808

ABSTRACT

Kelvin probe force microscopy (KPFM) was used to image austenitic stainless steel (SS) samples (Type 304L) fabricated by the laser engineered net shaping (LENS®) process. The samples were hydrogen charged (H-charged) and subsequently cut and polished. The surface contact potential difference (CPD) of the samples was measured using the KPFM technique, a form of atomic force microscopy. A set of uncharged samples was also studied for reference and changes in the CPD were on the noise level. For H-charged samples fabricated by the LENS® process, the resulting surface potential images show a change in CPD of about 10 – 20mV around cell-like boundaries (5–10 μm in size) and grain boundaries (50–100 μm in size). The significant change in the CPD is affected by variation of the local work function, which indicates the presence of hydrogen. The elemental composition of the LENS® samples was studied using energy dispersive spectroscopy (EDS) which showed an increase in the atomic percentage of Cr and a decrease in Ni around the cell-like boundaries. The existence of intercellular ferrite on the sub-grain boundaries may explain the propensity of hydrogen to segregate around these regions. The finer grain structure of LENS® samples compared to that of forged or welded samples suggests that the hydrogen can be dispersed differently throughout this material than in traditionally forged austenitic SS. This study is conducted to elucidate the behavior of hydrogen with respect to the microstructure of additively manufactured stainless steel alloys.

INTRODUCTION

Understanding the mechanism of hydrogen interactions in stainless steel (SS) is continually a topic of interest for applications which involve the long-term storage of hydrogen in SS vessels.[1] Atomic hydrogen in SS alloys segregates to regions of extended defects, such as grain and phase boundaries, and can cause stress and premature cracking through a process known as hydrogen embrittlement.[2,3,4] To develop and improve hydrogen storage and gas transfer systems, especially for hydrogen isotopes such as tritium, it is critical to understand the mechanisms of hydrogen embrittlement and to be able to co-locate the presence of hydrogen in the microstructural features of the metallic components.[5] For example, the presence of unwanted tritium is costly to gas handling

‡Oak Ridge Associated Universities Postdoctoral Appointee to Savannah River National Laboratory

processes due to tritium contributions to the waste stream and reduced efficiency of the recycling process.[6,7] The most common technologies for observing the effects of hydrogen in metals involve low-resolution optical microscopy and scanning electron microscopy of fracture surfaces (after mechanical testing), auto-radiography of tritium charged components, and transmission electron microscopy (TEM) which requires extensive preparation time.[8,9] Advanced microstructural imaging techniques, with minimal sample preparation needs, that are capable of resolving features down to the nanometer scale are needed.

Hydrogen segregated at the surface of SS samples and particularly at defect sites changes the local work function of the material and can be measured by Kelvin probe force microscopy (KPFM), a variant of atomic force microscopy (AFM).[10] KPFM produces surface potential (i.e., voltage) images, and is capable of measuring the local change in work function of surfaces with very high spatial resolution compared to current methods of optically imaging the microstructures. The spatial and energy resolution of KPFM is approximately 5 nm and 10 mV, respectively. [11] By locating the presence of hydrogen and its relationship with extended defects at the surface using KPFM, it may be possible to predict the long-term storage properties of a container.

The mechanism of Kelvin probe microscopy is based on establishing an electrical equilibrium between the work function of a metallized probe and the work function of a surface when the two systems are placed in electrical connection.[11] During KPFM operation, an AFM is used to bring an oscillating metallized probe very close to the sample surface. A piezo actuator mechanically drives the probe close to its resonant frequency, and, due to Van der Waals forces between the tip and surface, the resonance frequency of the probe changes as it raster scans across the surface of the sample for a predetermined scan area. In this way, topological variations can be measured. Simultaneously, the second resonant frequency of the probe is monitored while applying an AC voltage to electrostatically resonate the probe, and to cause an electrostatic force to develop between the probe and the surface. [11] Using a feedback loop, a specific DC voltage is also applied to the probe such that, at any given point on the surface, the electrostatic force between the tip and the sample is nullified. In the case of vanishing electrostatic force, the applied DC voltage will be equal to the surface potential. This value is called the contact potential difference (CPD), and is defined as the change in work function between the sample and the probe. [11]

KPFM has been previously used to image hydrogen in palladium thin films, duplex stainless steel and aluminum alloys.[12,13,14,15,16] Duplex stainless steels were electrochemically charged with hydrogen and subsequently measured with KPFM. Since the work function of the surface is the physical quantity being monitored during these measurements, it was possible to detect the diffusion of hydrogen to the surface as it changed the local work function. The ferrite phase showed a much more drastic change in work function compared to the austenite phase with increasing time of hydrogen loading. The change in work function was attributed to changes of the surface oxide band structure due to the presence of hydrogen.[13] Studying the behavior of hydrogen at the surface of duplex steels yields interesting results due to the vastly different diffusion rates of hydrogen in ferrite and austenite phases. Hydrogen segregation was also observed at deformation twin sites in twinning-induced plasticity (TWIP) steel, where the potential images showed a decrease in CPD in the region of the deformation twin sites. For most of the research reported in the literature, samples of stainless steel are coated with palladium to reduce topological effects, as well as to desorb the hydrogen. In these instances, the samples were electrochemically charged with hydrogen using various electrochemical solutions.

Additionally, it is important to characterize and understand the capabilities of additive manufactured (AM) stainless steel components being considered for hydrogen storage. Years of research and operational experience have demonstrated the effects of tritium on traditionally fabricated hydrogen service components, but the same cannot be said for AM components. KPFM studies of the microstructural behavior of hydrogen charged AM stainless steels can provide a technique to understand and predict the long-term effects of tritium and hydrogen embrittlement on its containers.

In this work, we discuss the results of KPFM imaging of AM stainless steel samples, and attempt to understand the behavior of hydrogen segregation in stainless steel.

EXPERIMENTAL METHODS

Four type 304L stainless steel (SS) samples were prepared by the directed energy deposition method of laser engineered net shaping (LENS®)[17] and are listed in Table 1. Hydrogen charging was performed on two of the samples (D and E) by pressurizing a chamber with 17 MPa of hydrogen gas at 350°C for approximately 2 weeks. These samples are hereafter called “H-charged” samples. After charging, samples were stored at 0°C to

prevent the unnecessary loss of hydrogen by diffusion. All four samples were cut and mechanically polished for AFM imaging by standard metallographic practices. Samples were cleaned by rinsing with soap and de-ionized (DI) water, followed by rinsing with ethanol and drying with dry nitrogen or air. A light electrolytic etch was performed with 10% oxalic acid for 30s at 10V to reveal the microstructures for initial measurements. Once these initial measurements were performed, the samples were re-polished to return to the as-polished conditions for subsequent analysis.

Table 1: Type 304L stainless steel samples fabricated by the LENS® process, and their charging conditions.

Name:	H-charged:
Sample C	No
Sample D	Yes
Sample E	Yes
Sample F	No

Imaging was performed using a Park Systems XE-70 AFM, in non-contact mode and the extended, electrostatic force microscopy mode coupled with a Stanford Research Systems lock-in amplifier for KPFM measurements. The AFM is contained within an environmental chamber to control the humidity levels, and dry nitrogen is flowing through the chamber during imaging. The relative humidity levels for the AFM measurements in this work are about 8%. Optical micrographs were taken on a Nikon MM-400 measuring microscope. Scanning electron microscopy (SEM) examination was conducted on a Hitachi SU823 SEM and energy dispersive spectroscopy (EDS) measurements were performed with the attached Oxford detector.

RESULTS

The surface morphology of the LENS® stainless steel samples was first characterized by optical microscopy after a quick electrolytic etching with oxalic acid was performed on the polished samples to reveal the grain features. **Figure 1** shows the microstructure for samples E and F. Typical microstructural patterns of the samples studied in this work are large grain features on the order of 50 – 100 μm across, and small cellular-like regions which are on average less than 5 μm. The cells have either polygonal (sometimes circular) shapes or elongated skeletal structures, and are contained within the large grains. The size of the structures is related to the heat input during melting and its corresponding solidification rate.

Samples fabricated by LENS® undergo highly localized heating from the laser, followed by rapid cooling and solidification as the heat source advances.[18, 19] This process creates fusion zone type microstructures very similar to those of welded samples. Each layer of the sample is melted by the laser, solidified rapidly, and followed by successive deposition and solidification of more material. The melt pools are about 500 μm to 1 mm wide, and AFM image areas are no greater than 45 μm, which allows each image to be fully contained within one melt region. As a result, cross sectional analysis of the samples with various orientations yields distinct microstructures. LENS® materials show very fine grains compared to forged steels and have directional anisotropy depending on the build parameters.[20] In order to view the fine microstructure, certain samples were electrolytically etched with 10% oxalic acid, and subsequently imaged using the AFM non-contact mode. The topographies of these samples are shown in **Figure 2**, where the detailed cellular [**Figs. 2(a)** and **2(b)**] and grain structures [**Fig. 2(c)**] can be clearly seen.

Surface potential measurements (KPFM), with their corresponding topography images, were performed on the as-polished samples, both H-charged and uncharged, to image the changes in the local work function across the LENS® samples, and are shown in **Fig. 3**. Uncharged samples (C and F) show very little variation in the surface potential images [**Figs. 3(e)** and **3(h)**], although subtle contrast seems to show grain boundaries. Large bright spots in the KPFM images for samples C and F indicate anomalous regions of locally varying work function that could be the result of surface contamination or contamination on the AFM probe.

In contrast, the KPFM images for the H-charged samples, D and E, show work function variations (bright regions) around the intercellular boundaries and around the grain boundaries [**Figs. 3(f)** and **3(g)**] with a change in the CPD of 10 – 20 mV. These images are representative of multiple images taken over the course of a year, with periodic re-polishing to achieve a pristine surface. EDS measurements were performed on all the samples, and the results for sample D are shown in **Fig. 4**, which are representative of the other samples. Both EDS line scans [**Figs. 4(c)** and **4(d)**] and maps [**Figs. 4(f)** and **4(g)**] show an increase in the Cr content and a decrease in the Ni content at the cellular and grain boundaries. This is indicative of retained ferrite at the boundaries of the austenitic microstructures, and is consistent with other studies on AM 316L stainless steel.[19] Thus, the regions of

increased H content are confined to the grain and cellular boundaries of the LENS® microstructures.

DISCUSSION

The fine grain structures of LENS fabricated materials are excellent candidates for understanding the nature of hydrogen segregation in stainless steel materials. Because of the finely varying microstructure, high resolution atomic imaging is capable of pinpointing the specific attributes that behave as hydrogen traps. Since KPFM is a surface sensitive technique, only the behavior of hydrogen at the surface can be investigated. However, the samples were cross-sectioned with different orientations with respect to the growth direction. As a result, morphologies with a texture dependence could be studied, although the results in this work do not reflect any texture dependence. Additionally, imaging the samples while in a nitrogen environment reduces the thin water layer which develops on the surface of materials exposed to ambient conditions and acts as a screening potential, which is detrimental to surface potential measurements.[21]

The KPFM images of the H-charged samples show bright regions around the cellular and grain boundaries which is caused by a change in the local work function. The Pt-coated metallized AFM probe acts as a vibrating capacitor as it is brought close to the surface, and is in electrical contact with the sample stage. A potential difference will develop between the sample and the probe due to differing Fermi levels, and will create an electrostatic force between the two materials. By applying a DC voltage (backing potential) to the probe, the electrostatic force between the probe and sample can be nullified. The CPD is defined as the change in work function between the two materials, and is equal in magnitude, opposite in polarity, to the backing potential that is necessary to nullify the electrostatic force between the sample and the probe. Precisely, CPD is defined as,

$$\mathrm{CPD} = \phi_{tip} - \phi_{sample} \quad (1)$$

where ϕ_{tip} and ϕ_{sample} are the work functions of the tip and sample, respectively. In this manner, very localized work functions can be measured, and attributed to the corresponding defects. It is important to mention that crystallographic orientation[22] and compositional variation will change the local work function as well, and the EDS data show that there is compositional variation in the same regions (e.g., grain boundaries)[18] which are posited to be attracting hydrogen. The studies on the uncharged samples show that changes in the work function due to crystallographic orientation or elemental variation must be below the detection of our instrumentation and setup, since the KPFM images of these samples show practically homogenous surface potential signals.

The exact cause of the work function variation due to hydrogen is debated. Early works on iron oxides assert that the surface work function variation comes from hydrogen permeating into the surface oxide layer, separating into a proton and its electron, thus reducing the oxide layer from Fe^{3+} to Fe^{2+} [23] and lowering its work function. However, if atmospheric oxygen is present, there is a likely chance that the surface can be reoxidized.[24] Another potential explanation is that the hydrogen diffusing to the surface causes lattice strain, which is in the form of tensile strain. Based on density functional theory and experiments performed on organic semiconductors, tensile strain should cause a decrease in the work function of the material, whereas compressive strain causes an increase in the work function.[25,26] The work function of the Pt probe is at least 6.10 ± 0.06 eV [27], although in air, it is expected to increase.[28] If an average value of the work function of austenitic stainless steel is roughly 4.5eV, then a decrease in the local work function would cause an increase in the CPD, as defined by Eq. (1). Indeed, an increase in the CPD is measured (as shown by the bright spots in the KPFM images of the H-charged samples), but whether it is caused by reduction of the iron oxide or strain fields from H segregation is uncertain. Since the samples in this work were stored in air for extended amounts of time, it is most likely that the slow reducing effect of hydrogen atoms percolating through the sample and into the surface oxide is compensated by the oxidative environment of the air, and the more likely cause of work function changes is due to strain caused by the presence of hydrogen.

Finally, it is interesting to speculate as to why hydrogen segregates to the intercellular regions and grain boundaries. Previous works show that the interaction of hydrogen with microstructural features in alloys plays an important role in an alloy's resistance to hydrogen embrittlement. [29] Also, permeation and diffusion studies show that hydrogen diffuses much more quickly from ferritic stainless steel than it does for austenitic steels. If the hydrogen is diffusing more quickly through the ferritic intercellular regions, it is possible that the rate at which it diffuses through the austenitic regions is much slower, and thus undetectable by the KPFM method. Further time-resolved studies must be performed to be certain in this regard. Additionally, thermal desorption measurements performed in conjunction with KPFM may shed light on the nature of the defects causing local variations in the surface work function.

CONCLUDING REMARKS

Austenitic stainless steels fabricated by the LENS technique were studied by KPFM and SEM techniques, in an attempt to understand the nature of hydrogen segregation in these materials which are intended for hydrogen storage. Characteristic LENS cellular and skeletal structures were observed, and EDS measurements showed that the boundaries of these regions had increased concentrations of ferrite stabilizing elements (i.e., Cr) material. KPFM measurements showed a change in the work function at these boundaries for the H-charged samples, but not for uncharged samples, which signifies that hydrogen has a propensity to segregate to grain boundaries and regions of retained ferrite.

ACKNOWLEDGMENTS

All work was performed at the Savannah River National Laboratory and sponsored by Savannah River Nuclear Solutions, LLC under Contract No. DE-AC09-08SR22470 with support from the U.S. Department of Energy, Laboratory Directed Research and Development (LDRD) program, as well as, support from the National Nuclear Security Administration (NNSA) Enhanced Surveillance and Advanced Materials Programs. The authors are grateful to T. Curtis for assistance with sample preparation, and to Sandia National Laboratory and Los Alamos National Laboratory for providing the LENS samples.

REFERENCES

[1] Caskey, Jr., G. R., Hirth, J. P., Oriani, R. W. and Smialowski, M., eds., Noyes Publication, Park Ridge, NJ, 1985, p. 822.

[2] Koyama, M., Rohwerder, M., Tasan, C. C., Bashir, A., Akiyama, E., Takai, K., Raabe, D. and Tsuzaki, K. "Recent progress in microstructural hydrogen. mapping in steels: Quantification, kinetic analysis, and multi-scale characterisation," *Mater. Sci. Technol.* **33** (13), 1481 (2017).

[3] Perng, T.-P. and Altstetter, C. J., "Hydrogen effects in austenitic stainless-steels," *Mater. Sci. Eng. A*, **129**(1), 99 (1990).

[4] Wang, Y., Wang, X., Gong, J., Shen, L. and Dong, W., "Hydrogen embrittlement of catholically hydrogen-precharged 304L austenitic stainless steel: Effect of plastic pre-strain," *International Journal of Hydrogen Energy*, **39**(25), 13909 (2014).

[5] Daw, M. S. and Baskes, M. I., "Semiempirical, quantum mechanical calculation of hydrogen embrittlement in metals," *Phys. Rev. Lett*. **50**, 1285 (1983).

[6] E. A. Clark, Decontaminating and Melt Recycling Tritium Contaminated Stainless Steel,", Report # WSRC-TR-95-0160, Westinghouse Savannah River Co., Aiken, SC (United States) (1995).

[7] Perevezentsev, A., Watanabe, K., Matsuyama, M. & Torikai, Y., "Contamination of Stainless Steel Type 316 by Tritium," *Fusion Science and Technology*, **41**(3P2), 746 (2017).

[8] Tosten, M. H. and Morgan, M., "Transmission electron microscopy study of helium-bearing fusion welds," *Proc. Internatl. Hydrogen Conf. - Effects of Hydrogen on Materials*, p.694 (2009).

[9] K. J. Imrich, M. J. Morgan and M. H. Tosten, "Extraction of Fracture-Mechanics and Transmission-Electron-Microscopy Samples from Tritium-Exposed Reservoirs using Electric-Discharge Machining," Savannah River National Laboratory, Aiken, SC. WSRC-STI-2006-00125, Rev. 1, (2006)..

[10] Koyama, M., Bashir, A., Rohwerder, M., Merzilikin, S. V., Akiyama, E., Tsuzaki, K. and Raabe, D., "Spatially and Kinetically Resolved Mapping of Hydrogen in a Twinning-Induced Plasticity Steel by Use of Scanning Kelvin Probe Force Microscopy," *J. Electrochem. Soc*. **162**, C638 (2015).

[11] Melitz, W., Shen, J., Kummel, A. C. and Lee, S., "Kelvin Probe Force Microscopy and Its Application," *Surf. Sci. Rep*. **66**, 1 (2011).

[12] Evers, S., Senoz, C. and Rohwerder, M., "Spatially resolved high sensitive measurement of hydrogen permeation by scanning Kelvin probe microscopy," *Electrochemica Acta* **110**, 534 (2013).

[13] Senoz, C, Evers, S., Stratmann, M. and Rohwerder, M., "Scanning Kelvin Probe as a highly sensitive tool for detecting hydrogen permeation with high local resolution," *Electrochem. Commun*. **13**, 1542 (2011).

[14] Evers, S., Senoz, C. and Rohwerder, M., "Hydrogen Detection in Metals: a Review and Introduction of a Kelvin Probe Approach," *Sci. Technol. Adv. Mater*. **14**, 014201 (2013).

[15] Larignon, C., Alexis, J., Andrieu, E., Lacroix, L., Odemer, G. and Blanc, C., "Investigation of Kelvin Probe Force Microscopy Efficiency for the Detection of Hydrogen Ingress by Cathodic Charging in an Aluminium Alloy," *Script. Mater.* **68,** 479 (2013).

[16] An, B., Hua, Z., Iijima, T., Gu, C., Zheng, J., Marchi, C. S., "Scanning Kelvin Probe Force Microsopy Study of Hydrogen Distribution and Evolution in Duplex Stainless Steel" *Proceedings from the ASME Pressure Vessels and Piping Conference*, Waikoloa, Hawaii, PVP2017-66121, (2017).

[17] Korinko, P. S., Adams, T. M., Malene, S. H., Gill, D. and Smugeresky, J., "Laser Engineered Net Shaping® for Repair and Hydrogen Compatibility," *J. Welding*, **90**, 171 (2011).

[18] Wang, Z., Palmer, T. A. and Beese, A. M., "Effect of processing parameters on microstructure and tensile

properties of austenitic stainless steel 304L made by directed energy deposition additive manufacturing," *Acta Mater*. **110**, 226 (2016).

[19] Ziętala, M., Durejko, T., Polański, M., Kunce, I. , Płociński, T., Zieliński, W., Łazińska, M., Stępniowski, W., Czujko, T., Kurzydłowski, K. J., Bojar, Z., "The microstructure, mechanical properties and corrosion resistance of 316 L stainless steel fabricated using laser engineered net shaping," *Mater. Sci. Eng*. *A*, **677**, 1 (2010).

[20] Wei, H. L., Mazumder, J. and DebRoy, T. "Evolution of solidification texture during additive manufacturing," *Sci. Rep*. **5**, 16446, (2015).

[21] Burgstaller, W., Schimo, G., Hassel, A. W., "Challenges in hydrogen quantification using Kelvin probe technique at different levels of relative humidity," *J. Solid State Electrochem*. **21**, 1785 (2017).

[22] Hua, Z., An, B., Iijima, T., Gu, C. and Zheng, J. "The finding of crystallographic orientation dependence of hydrogen diffusion in austenitic stainless steel by scanning Kelvin probe force microscopy," *Scripta Mater*. **131**, 47 (2017).

[23] Krasemann, M., Streckel, H., Hoffman, K., Grabke, H. J. and Stratmann, M., "Detection of Hydrogen Ingress into Iron Oxide and Iron Oxy-Hydroxide Layers by Kelvin Probe," Electrochem. Soc. Proc. **97**(26), 207 (1998).

[24] Williams, G., McMurray, H.N., Newman, R.C., "Surface oxide reduction by hydrogen permeation through iron foil detected using a scanning Kelvin probe," *Electrochem. Comm*. **27**, 144 (2013).

[25] Wang, X. F., He, L., Halas, S., Pieńkos, T., Lin, J. G. and Durakiewicz, T., "The canonical work function-strain relationship of the platinum metal: A first-principles approach to metal-gate transistor optimization," *Appl. Phys. Lett*. **102**, 223504 (2013).

[26] Wu, Y., Chew, A. R., Rojas, G. A., Sini, G., Haugstad, G., Belianinov, A., Kalinin, S. V., Li, H. , Risko, C., Brédas, J-L., Salleo A. & Frisbie, C. D., "Strain Effects on the Work Function of an Organic Semiconductor," *Nat. Commun*. **7**, 10270 (2016).

[27] Derry, G. N. and Ji-Zhong, Z. "Work function of Pt (111)," *Phys. Rev. B*. **39**(3), 1940 (1989).

[28] Chaston, J. C. "Reaction of Oxygen with the Platinum Metals," *Platinum Metals Rev*., **8**(2) 50, (1964).

[29] Somerday, B. P. and Sefronis, P. International Hydrogen Conference (IHC 2016): ***Materials Performance in Hydrogen Environments***. (ASME, 2017).

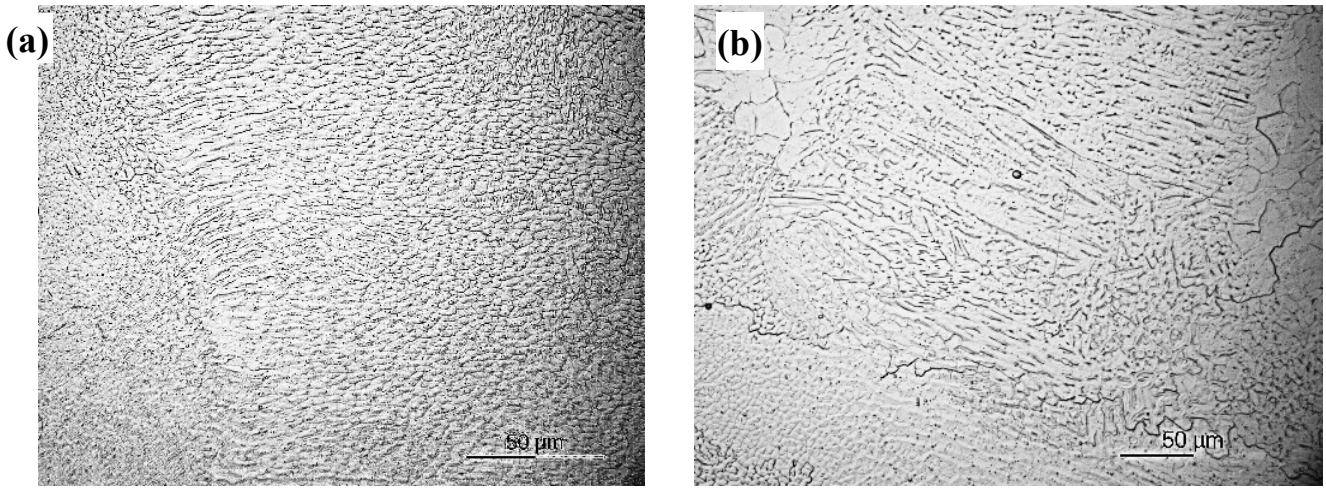

Figure 1: Optical micrographs (500x zoom) of samples (***a***) E and (***b***) F after a light oxalic etch. The varying microstructure consists of large grains, and fine cellular structures.

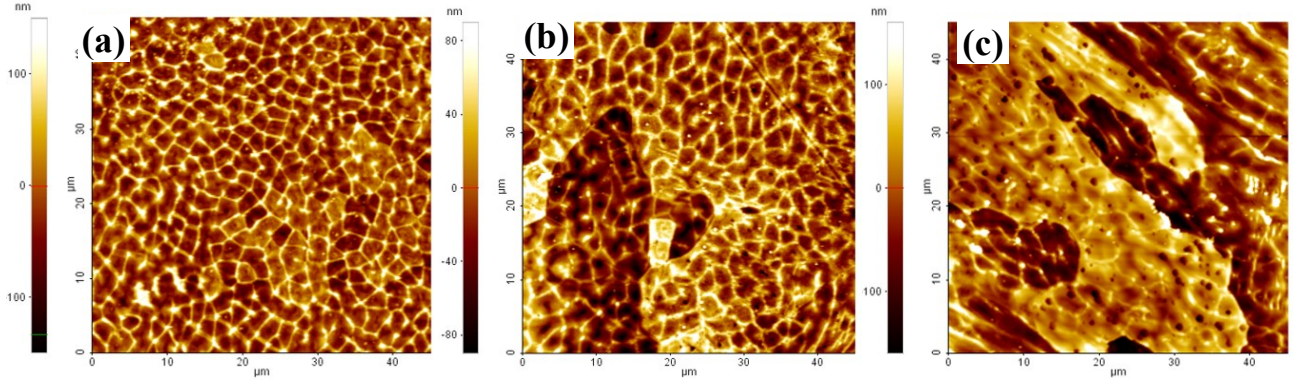

Figure 2: AFM topography images of samples E (***a***) and (***b***), and sample F (***c***) after 30s electrolytic etching with 10% oxalic acid.

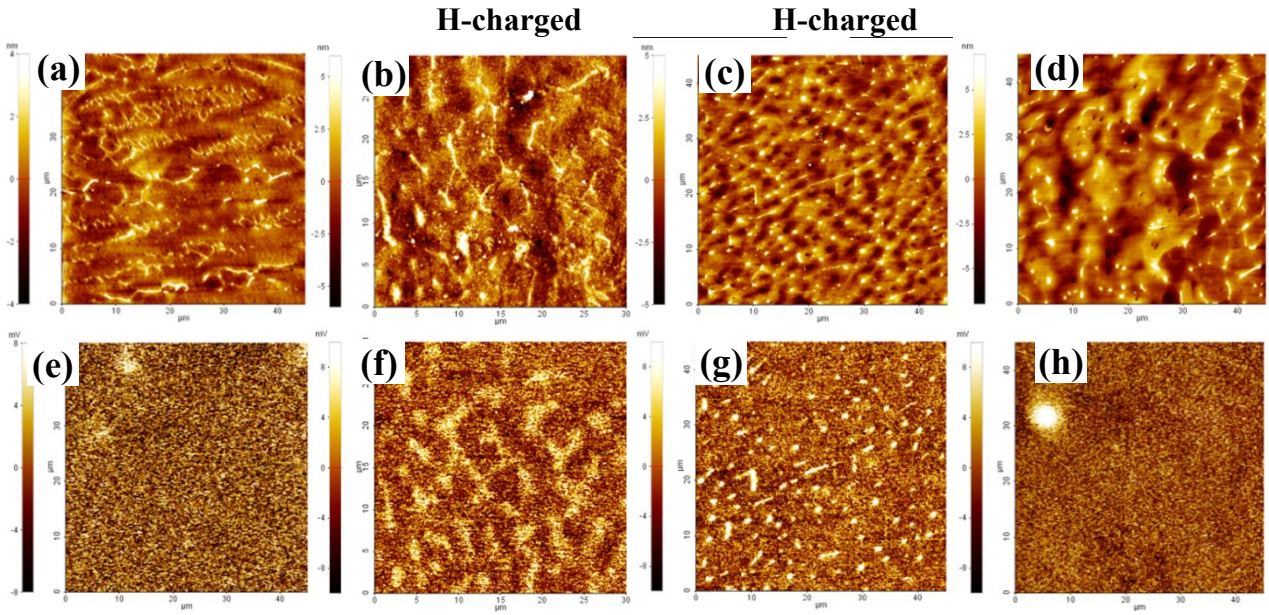

Figure 3: (***a***)-(***d***) Topography images of sample C, D, E, and F, respectively, and the corresponding KPFM images (***e***)-(***h***).

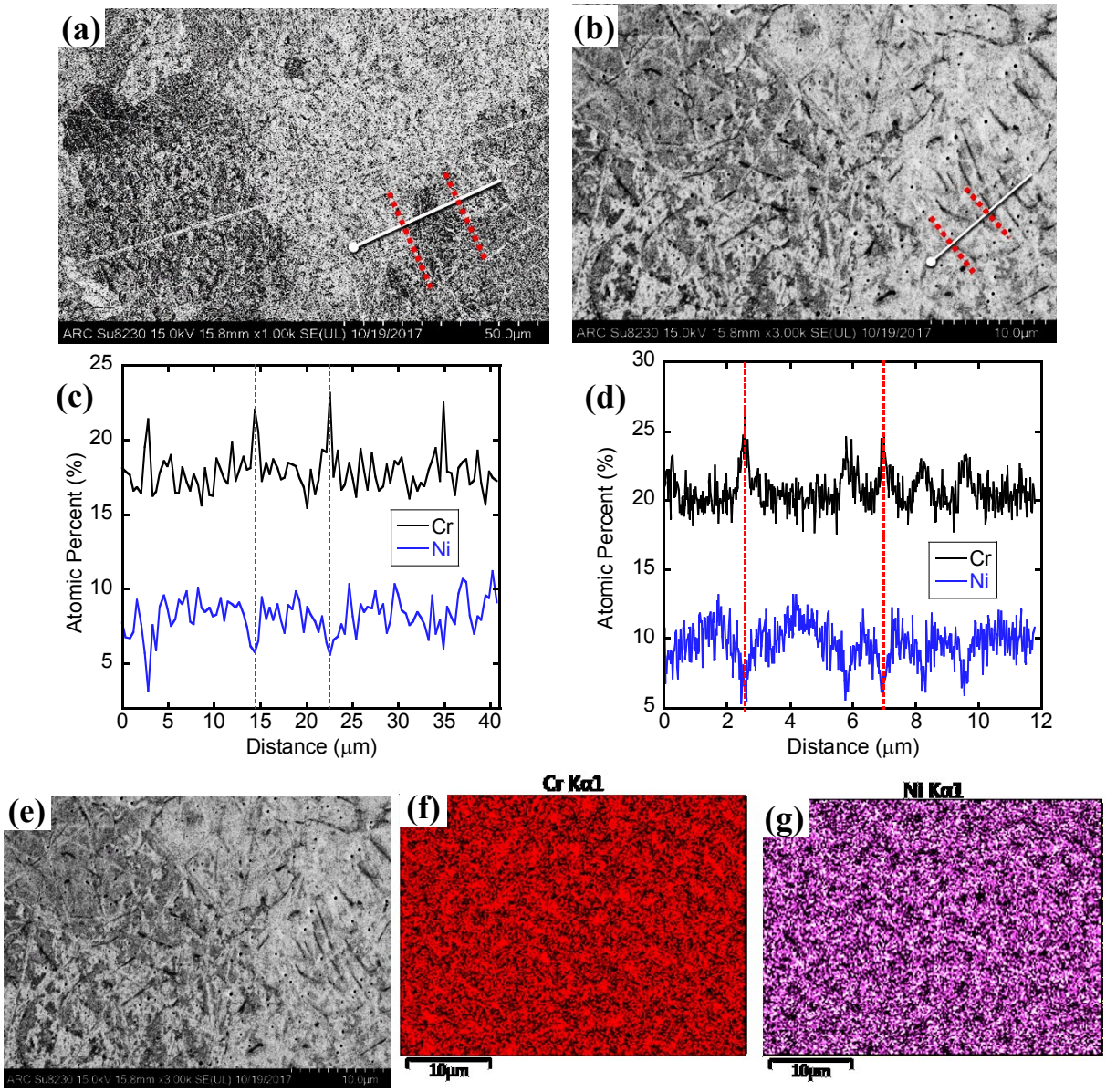

Figure 4: SEM micrographs, EDS line scans, and EDS maps of sample D. The red dotted lines in (***a***) highlight the edges of a grain, and the correlating EDS line scan (***c***) shows an increase in Cr and decrease in Ni content. Similarly, (***b***) and (***d***) show an increase in Cr and decrease in Ni content at the boundaries of the rice-like structures, which are similar to cellular structures in these LENS materials. (***e***)-(***g***) corresponding EDS maps.